Widening global variability in grassland biomass since the 1980s

A list of authors and their affiliations appears at the end of the paper

Global change is associated with variable shifts in the annual production of aboveground plant biomass, suggesting localized sensitivities with unclear causal origins. Combining remotely sensed normalized difference vegetation index data since the 1980s with contemporary field data from 84 grasslands on 6 continents, we show a widening divergence in site-level biomass ranging from +51% to −34% globally. Biomass generally increased in warmer, wetter and species-rich sites with longer growing seasons and declined in species-poor arid areas. Phenological changes were widespread, revealing substantive transitions in grassland seasonal cycling. Grazing, nitrogen deposition and plant invasion were prevalent in some regions but did not predict overall trends. Grasslands are undergoing sizable changes in production, with implications for food security, biodiversity and carbon storage especially in arid regions where declines are accelerating.

Shifting annual production of aboveground peak biomass by vascular plants (hereafter 'biomass') has been observed worldwide in response to global environmental change[1–5]. These shifts differ in magnitude and direction including positive responses (that is, 'winners and losers'[6]) suggesting localized sensitivities that have been difficult to simultaneously measure and test[7–11]. Given the importance of biomass to humanity for food and fuel and the likelihood of intensifying consumption going forward, there is an urgent need to assess its vulnerability to global change especially in areas where yield declines could intensify[12,13].

Analyses to date on biomass shifts[13–15] have mostly relied on remotely sensed data that can be prone to estimation bias and an inability to discern underlying fine-scale drivers[9–16]. This is problematic because plant biomass often varies with combinations of coarse- and fine-scale factors whose interactions can be expressed uniquely by location, even when vegetation structure and climate may seem similar[8,16]. For example, anthropogenic nitrogen deposition and plant invasion can sometimes dramatically increase biomass especially with warming[17–19], yet some global regions are largely unaffected by one or both factors.

To date, hypothesized drivers of biomass variability have emphasized combinations of climate change, phenological shifts, nitrogen deposition or local-scale biotic interactions. Climate effects on biomass can vary based on regional differences in the magnitude of temperature change relative to historic baselines (for example, greater warming at higher latitudes), shifts in seasonality within and across years (for example, longer, hotter summers), the magnitude of temperature change relative to the tolerance thresholds of local taxa, and interactions between temperature and precipitation including whether warming sites become wetter or more arid[20,21]. Phenologically, shifts in the timing of seasonal growth can have variable effects on plant biomass[8,9,15]—earlier emergence can increase biomass if plants are biologically active for longer periods or reduce it by accelerating seasonal cycling such that growing seasons shorten[22]. The effects of anthropogenic nitrogen deposition on plant biomass and diversity sometimes exceed those of climate and vary by proximity to centres of industry and agriculture[19]. Nitrogen deposition often interacts strongly with climate, given linkages among moisture availability, growing period and nitrogen demand by plants[19,23]. Finally, a multitude of biotic factors can affect biomass differently by location, including among-site variation in plant species richness[24], the diversity of plant traits[25], levels of plant invasion[17] and overgrazing[26,27]. As expected, given these diverse and often scale-dependent drivers of biomass change, their effects have been difficult to disentangle. Doing so will require a global-level systematic assessment of biomass regulation both within and among continents[28,29].

Here we link long-term remotely sensed normalized difference vegetation index (NDVI) data with more contemporary plot data from 84 grasslands on 6 continents to test drivers of biomass variability in response to global change. These grasslands span a latitudinal gradient

from −52° to +78° (four within tropical latitudes) and capture ~1.6% of the world's total non-woody vascular flora including ~5% of all Poaceae and ~3% of Cyperaceae (Supplementary Table 1). Seventy per cent of our sites are arid (potential evapotranspiration (PET) > annual rainfall; Supplementary Table 1), matching the ratio of arid-to-mesic grasslands globally[30], with the highest number of sites in North America (41 sites), followed by Europe (17), Australia (13), South America (6), Africa (4) and Asia (3) (Supplementary Fig. 1). We classify 'grasslands' as low-statured unforested plant communities. Functionally, grasslands occupy a climatically and edaphically determined tension zone between forest and desert[29–31], regulated by climate seasonality, extreme weather, fire, and human-managed and natural grazing with its total area covering ~53 million km^2 globally (excluding Antarctica and Greenland). These regulating processes are associated with variability in grassland production, especially relating to climate[32–34]. These same processes are being fundamentally reshaped by global environmental change, resulting in grasslands becoming a bellwether of resilience (or vulnerability) to anthropogenic transformation including shifts in biomass.

Our remotely sensed data track changes in annual peak biomass from as early as 1986 based on Landsat-derived peak NDVI. Our primary analyses focused on identifying drivers of change in peak NDVI using temporal factors measured during the same interval (1986–2020). These included changes in the timing of three NDVI-based phenophases that can affect peak biomass: vegetation emergence (that is, start-of-season spectral greening), senescence (that is, end-of-season spectral browning) and growing season length (GSL, duration from greening to browning), as well as inter-annual and inter-seasonal changes in temperature, precipitation and PET[35]. We also tested NDVI trends in relation to site-level baseline factors calculated from different durations including mean annual precipitation and mean annual temperature based on hourly modelled temperature data from 1970 to 2020, and site aridity (the ratio of annual PET to precipitation, 1970–2020). Other baseline factors were anthropogenic nitrogen deposition based on modelled data from 2014 to 2016[36], the number of plant species per site based on the net total of all species detected in the first 5 years of sampling starting as early as 2007, the percentage of exotic taxa found in each site-level species pool over 5 years of sampling[29], grazing impacts by large mammals determined using offtake comparisons with exclosures at a subset of 46 grasslands, and composite community-level measures of plant traits for the species present at each site[37]. Using the aboveground biomass of plants (that is, combined live, litter and non-vascular) annually sampled starting as early as 2007, we examined the accuracy of satellite-derived NDVI in predicting grassland biomass, given that there can be estimation biases relating to latitude, elevation or species richness[9,16]. Analytically, we tested drivers of remotely sensed peak grassland NDVI by evaluating a series of regression and multivariate models that isolate localized differences based on our various explanatory factors (Table 1).

Table 1 | Major factors associated with changing mean in peak NDVI in 84 grasslands, 1986–2020

Parameter	Estimate	s.e.m.	*Z* score	*P* value
Intercept	0.0018	0.0002	11.48	**<0.0001**
GSL	0.0021	0.0003	6.13	**<0.0001**
GSL × temperature change	−0.0037	0.0008	4.5	**<0.0001**
Aridity × temperature change	−0.0024	0.0007	3.14	**0.002**
Temperature change	0.0010	0.0004	2.50	**0.013**
GSL × species richness	0.0018	0.0008	2.38	**0.018**
Temperature change × species richness	0.0020	0.0009	2.17	**0.03**
Aridity	−0.0007	0.0003	2.14	**0.033**
Species richness	−0.0004	0.0003	1.27	0.2
Percentage of exotic species	−0.0002	0.0003	0.54	0.59
Aridity × species richness	0.0003	0.0007	0.41	0.68
Precipitation change	0.0001	0.0002	0.33	0.74
Precipitation change × temperature change	−0.0002	0.0007	0.31	0.76
Elevation	0.00000	0.0002	0.25	0.80

Shown are variables that are significant drivers of changing NDVI (in bold) and the remaining non-significant variables retained in the model selection process. Hypothesized factors that are not listed (for example, nitrogen deposition) were not detected as influential, even non-significantly, during model selection.

Results and discussion

We observed a fourfold divergence in the slope of change in annual NDVI-estimated biomass over the past several decades (Fig. 1). This amounted to biomass shifts ranging from a maximum gain of 51% to a 34% decline (Fig. 1 and Supplementary Fig. 1). Overall, 56% of sites increased significantly, especially in the Arctic, the Pacific Northwest of North America and western Europe. Other sites from both hemispheres declined, all of which were arid, including grasslands in Australia, Argentina and parts of central and southwestern North America especially California. Of the grasslands, 36% showed no significant shift in biomass, regardless of phenological change, warming, altered precipitation, nitrogen deposition or plant invasion. Such geographically variable long-term changes in non-woody NDVI-estimated grassland biomass, including both sizeable increases[14,38–42] and declines even within the same continent (Supplementary Figs. 1 and 2), are consistent with previous observations especially from the Arctic[9,10,15]. We report this variability to be a global phenomenon affecting many grasslands.

We found that variability in shifting NDVI-estimated biomass was primarily explained by increases in growing season length, especially in combination with warming (Fig. 2, Supplementary Figs. 2 and 3, and Table 1). Between the late 1980s and the late 2010s, growing seasons increased by an average of 9 days (1986–1990: $\bar{x}$ = 157 days (s.e.m. = 3); 2016–2020: $\bar{x}$ = 166 days (s.e.m. = 2)). In total, 87% of sites had significant changes in the timing of the onset of greening, the onset of browning and/or the length of the growing season since 1986 (Supplementary Fig. 4), indicating that many grasslands globally are undergoing substantive shifts in seasonal cycling. Longer growing seasons have been implicated as a warming response in grasslands and some cropping systems, and a causal factor of increased biomass based on the assumption that plants are active for longer periods[22]. Conversely, advancing greening, elevated production or moisture limitation in arid environments can sometimes accelerate leaf physiological processes relating to photosynthesis that, in turn, shorten the growing season by triggering earlier senescence[22,23]. In total, 39% of sites had both earlier emergence and delayed senescence, thereby creating longer growing seasons (Supplementary Fig. 4)—it was these grasslands with the longest growing seasons that tended to have the largest increases in NDVI-estimated biomass. However, many other sites responded differently such that there was no consistent global relationship between changes to the timing of emergence and senescence (that is, starting earlier does not predict the timing of senescence: $F_{1,83} = 0.95$, $P = 0.33$; Supplementary Fig. 4). For example, 19% of sites with earlier emergence in spring experienced earlier spectral browning, thereby shortening the growing season, which has been observed previously in arid areas[23] and parts of the Arctic[43,44] including sites analysed in this study. In total, variability in the connection between shifting phenology and changes in peak biomass shows that there can be not only powerful global trends in grassland responses to environmental change (for example, longer growing seasons at many sites) but also localized and divergent outcomes sometimes regulated by different factors.

All sites showed temperature increases since the mid-1980s (that is, all 84 temporal slopes for temperature were positive; Supplementary

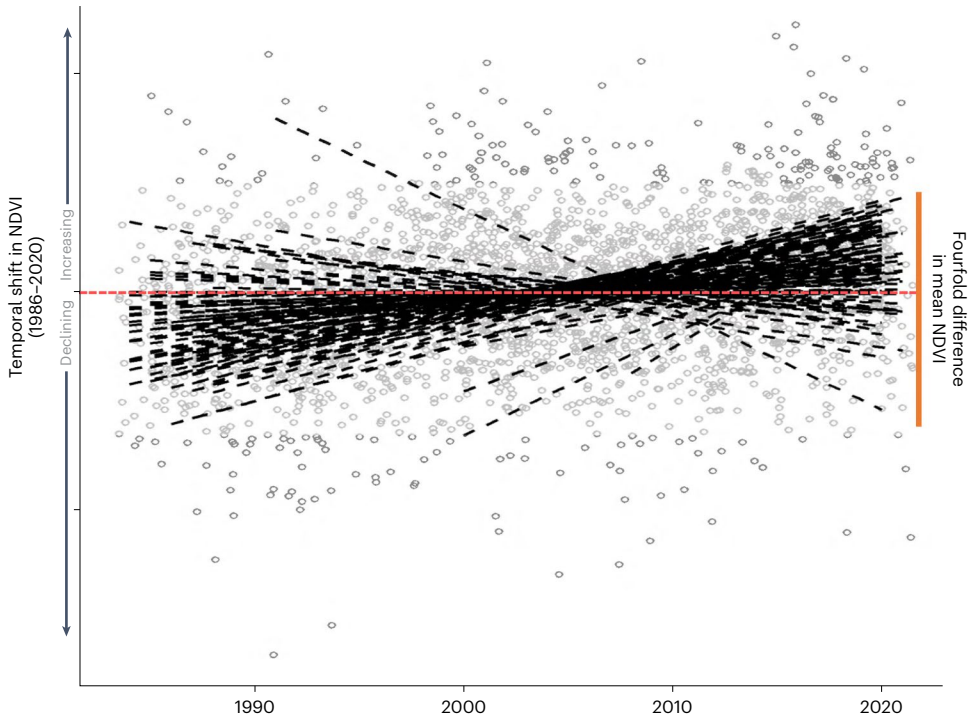

Fig. 1 | Temporal change in mean peak NDVI. Fitted trend lines for 84 grasslands, with the red dashed line indicating no temporal change. The open circles are the peak NDVI measures for each grassland over time (n = 2,856). In total, 56% of sites have significant positive increases while 5% have significant declines, resulting in a fourfold difference in mean peak NDVI change. Given the wide spread of points and the risk of outlier bias, our fitted trends derive from a linear model using a Theil–Sen median regressor. Plotted trend lines were obtained from this model and filtered based on P values from a Mann–Kendall trend test (Methods).

Figs. 5 and 6). However, the effects of warming on growing season length were not universal but instead depended on the distinction between sites with the highest temperature increases but relatively low MATs (for example, the Arctic, Patagonia and the alpine steppes of the Mongolian and Tibetan Plateaus) versus those with the highest MATs but less overall warming (for example, arid grasslands of Australia, southwestern North America, Africa and South America) (Supplementary Figs. 2–6). The former were more often in the Northern hemisphere, in line with observations that global warming to date has been more pronounced north of the equator (that is, interhemispheric temperature asymmetry[45]) (Fig. 3 and Supplementary Fig. 6). These sites with the highest warming also tended to be characterized by both high MAP and large increases in annual rainfall—the wettest sites generally are becoming both wetter and warmer. This is consistent with the ability of warmer air to support more moisture, as has been observed with increasing snowfall in a warming Arctic[43]. Conversely, sites with higher baseline MATs, less warming and reduced NDVI were all arid grasslands that tended to undergo a shortening of growing season length, usually relating to an earlier onset of spectral browning in summer (Supplementary Figs. 6 and 7). Not all arid sites experienced declining biomass—only 32% of 59 arid sites had negative temporal slopes in NDVI even though 58% of all sites had less precipitation, increases in PET or both (Supplementary Figs. 1, 6 and 7).

Our observed warming trends were more seasonal than annual, especially in the spring and summer months—this contributed to the tight connection between growing season length and temperature (Supplementary Fig. 2). We examined changes to seasonal and annual temperatures by site from 1986, which is near the beginning of Landsat data collection, while also capturing the onset of accelerating contemporary planetary warming that continues to the present day[34,43]. In testing the magnitude of seasonal and annual changes, we found that seasonal changes were more prevalent, with 37% of sites having significantly warmer spring temperatures and 47% having warmer summers (Supplementary Fig. 8). By contrast, only a subset of sites had significant increases in annual warming despite all slopes being positive. This decoupling of frequent seasonal warming from less common significant annual warming suggests an intensification of within-year inter-seasonal differences as has been reported previously in grasslands, with periods of increasing temperature in some seasons being muted or offset by cooling at other times of the year[6,46]. For example, we observed cooling spring temperatures in numerous mid-latitude grasslands of central North America and western Europe (Supplementary Fig. 8)—many of these sites had increasing NDVI.

We also saw significant influences of species richness on changes in peak NDVI, although always interacting with phenology or climate (Table 1). Among sites with lengthening growing seasons or warming temperatures, species-rich grasslands generally showed greater increases in NDVI than species-poor sites (Table 1 and Supplementary Figs. 2 and 9). Conversely, for grasslands with shortened growing seasons or less warming (for example, high-MAT sites from the Southern hemisphere and California), those with below-average richness were predicted to show reduced or less pronounced NDVI increases. These outcomes indicate some form of context-dependent functional complementarity, which would be consistent with the intertwined causal factors known to regulate diversity and biomass in grasslands[47–49]. They also reveal an absence of any independent relationship of richness (Fig. 2 and Supplementary Fig. 9), and indeed, sites with the highest numbers of species (for example, the African Serengeti) did not necessarily show increasing NDVI. Such complexities on how richness affects biomass are illustrated when considering the numbers of invasive grassland plants at our sites. Invasion is sometimes linked with large increases in community-level biomass and site-level richness[50], yet we observed the opposite responses—invaded grasslands were more likely to have declining biomass and fewer species. This probably reflects

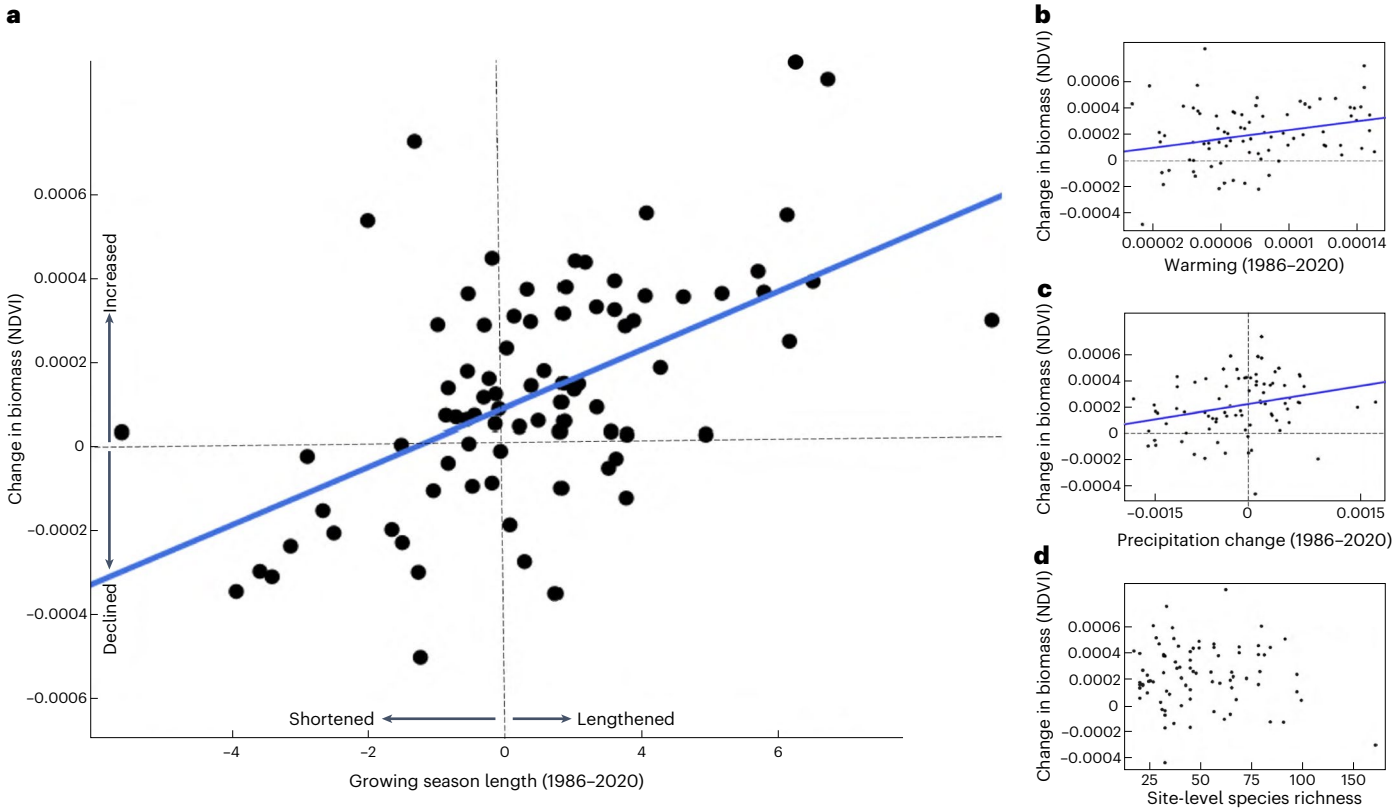

Fig. 2 | Relationship between changes in major explanatory factors and maximum NDVI. a, The figure emphasizes the significant effect of changes in growing season—shortening (left) or lengthening (right)—on shifts in grassland biomass declines (bottom) or increases (top) estimated with remote-sensed NDVI ($F_{1,83}$ = 31.8; P < 0.0001). The units for the change in biomass (NDVI) are the regression slopes. **b**,**c**, There are also significant relationships between increasing NDVI and the slope of temperature increase by site ($F_{1,83}$ = 6.6; P = 0.012; note: all sites warmed) (**b**) and increasing NDVI and the slope of changes in annual precipitation ($F_{1,83}$ = 5.3; P = 0.023) (**c**). **d**, For species richness, there was no univariate effect on changing NDVI ($F_{1,83}$ = 0.34; P = 0.56), although it interacted significantly with growing season length and warming (Table 1 and Supplementary Fig. 9). The inserted dashed lines in **a**–**c** indicate areas of no net change. All tests are linear regressions among the 84 sites of this study.

climatic factors—most invaded sites were in arid regions where biomass trends since the 1980s were non-significant or negative. It also probably reflects lower numbers of species—sites dominated by invasive plants had significantly fewer plant taxa ($F_{1,63}$ = 9.2, P = 0.004).

Several of our non-temporal hypothesized factors had no detectable effects on changes to grassland NDVI despite often having sizable effects on biomass at some sites (Table 1). Sites with high levels of nitrogen deposition, especially in eastern North America, higher-elevation areas of western Europe, and areas of China (Fig. 3), did not show significant changes in NDVI despite the well-described impacts of anthropogenic nitrogen increasing grassland biomass[19]. Similarly, there was a lack of detectable association between sites with high grazing offtake and changes to NDVI (Supplementary Table 2). As with nitrogen deposition, grazing can significantly affect grassland biomass[26] and, indeed, some of our grasslands have substantive differences in biomass between grazed and fenced areas including mesic grasslands of the Northern hemisphere (sheep meadows in the UK, reindeer barrens in Finland) and arid regions of Australia[51,52]. However, variation in levels of offtake estimated by our exclosures was unable to predict the likelihood of NDVI change relative to the global-scale impacts of phenology, climate or species richness (Supplementary Table 2). Finally, we also failed to detect associations between site-level biomass change and variability in community-wide aggregate measures of plant size (for example, leaf area index (LAI), height) or foliar nutrients despite a wider spectrum of resource-foraging strategies in plants sometimes being connected to higher biomass[37] (Supplementary Table 3). Of particular note in our study was a lack of association between biomass change and LAI. Remotely estimated LAI is often used to model plant production given the strong connection between canopy density, light capture and biomass[53,54]. However, we observed no predictive relationship between community-level LAI and long-term shifts in NDVI despite 90-fold differences in canopy density ranging from sparse arid grasslands of Australia and the American southwest to dense high-elevation mesic grasslands of the European Alps (Supplementary Table 3).

Combined, the prevalence of grasslands with trends towards higher site-level biomass created a net 13.6% increase among our 84 sites since the 1980s (Fig. 1; $F_{1,83}$ = 91.6, P < 0.0001). Longer-term increases in biomass were also detected using our field-measured data (Fig. 4 and Supplementary Fig. 10) and aligned with other reports of increasing overall plant biomass with global environmental change[38–42]. That being said, this magnitude of increase could be viewed with caution. In total, 61 of our 84 sites are located in the Northern hemisphere, especially North America and Europe, where increases in precipitation and biomass are known to be especially pronounced[55,56]. Furthermore, there is evidence of a threshold of ~500 mm per year in precipitation below which sensitivity to climatic variability intensifies[56]. Although most of our sites are arid (PET > MAP), their annual precipitation averages 790 mm (s.e.m. = 43), with only 25% falling below 500 mm. We tested the potential effects of these factors on the subset of sites that are arid or have MAP levels <500 mm, and still observed net increases in biomass (arid sites: +12.2% (s.e.m., 2.6%); MAP < 500 mm: +15.6% (s.e.m., 5.7%)). Nonetheless, we might still anticipate that mean site-level increases in biomass would be lower if more of our sites occurred in areas where declining precipitation is especially pronounced.

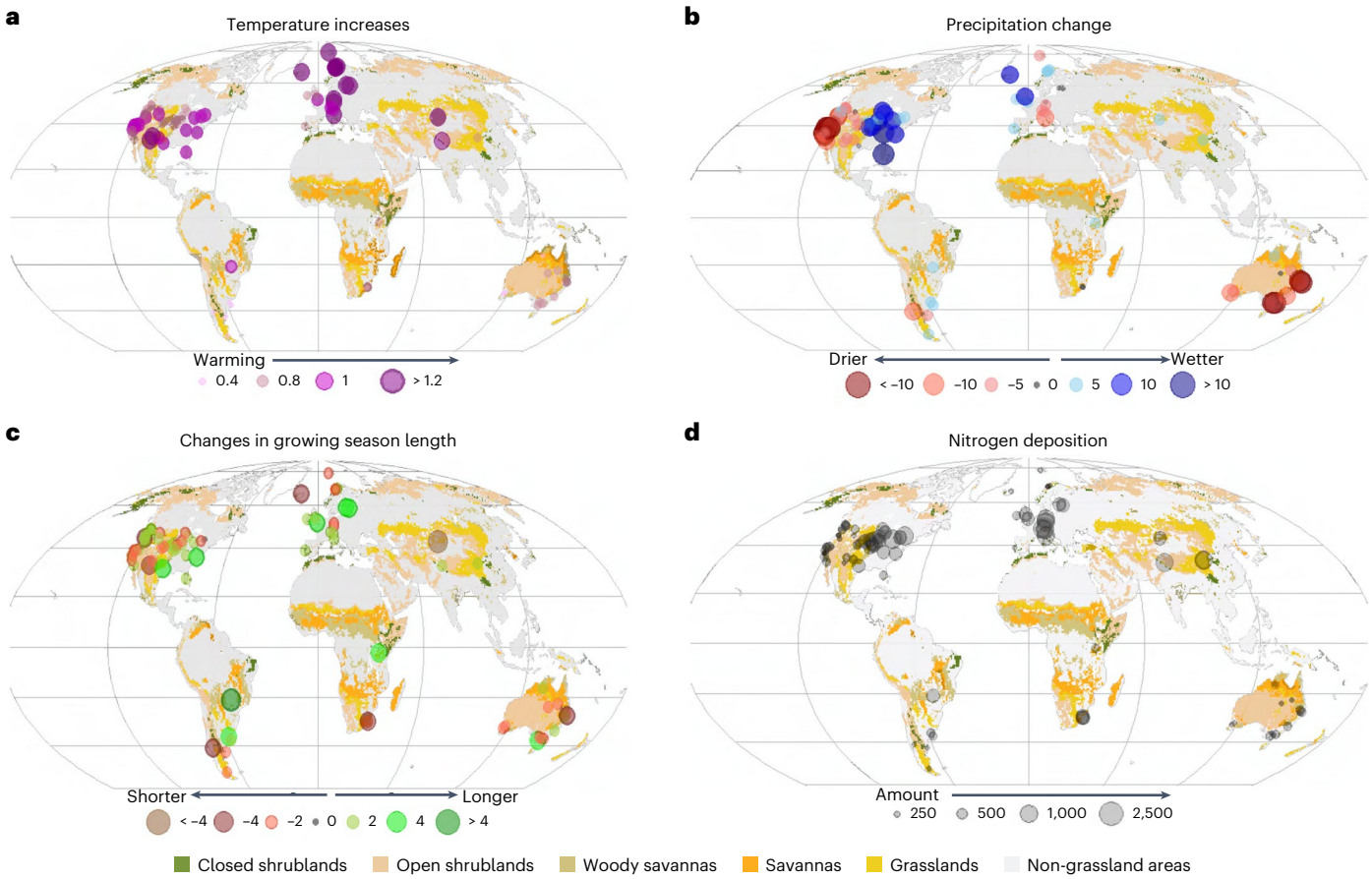

Fig. 3 | Global maps showing variation among sites in various conditions. **a**, Shifting average annual temperature. Data for temperature and precipitation were obtained from the Climatic Research Unit (CRU)[35]. The largest temperature increases are mostly in the Northern hemisphere—Southern hemisphere sites have higher MATs but lower levels of warming since the 1980s. **b**, Average annual precipitation. **c**, Growing season length for 1986–2020, derived by site and over time based on differences between remotely sensed spectral greening and spectral browning each year. **d**, Levels of atmospheric nitrogen deposition modelled for 2014–2016, estimated using the GEOS-Chem Chemical Transport Model[36], which estimates wet and dry deposition of inorganic nitrogen using models of atmospheric chemistry together with meteorological data and emission data. These nitrogen data have a 2° × 2.5° resolution.

Biomass variability is not unexpected in grasslands, given its regulation by combinations of factors whose relative importance can change by locale including supply rates of limiting nutrients, grazing pressure and whether warming increases or suppresses plant growth depending on precipitation[31–34]. Indeed, localized responses in biomass depending on whether warming sites are getting wetter or drier also occur in annual crops[6], which is expected given that large percentages of the world's croplands were once grassland[11,57]. In addition, previous work on global-scale shifts in NDVI-derived estimates of biomass, including in grasslands, has shown both increases and decreases since the 1980s without a consistently clear mechanistic understanding given the challenges of testing fine-scale processes[1,2,14,58]. Here we consolidate the disparate findings of previous work by showing that localized differences emerge because the dominant regulatory processes appear to vary widely. These findings are evident even though our results probably underestimate the full extent of shifting grassland biomass with global change since the 1980s. For example, we do not account for increased biomass caused by the invasion of trees and high-statured shrubs into grassland—an increasingly prevalent phenomenon[9,59]. We also did not account for shifts in root biomass, with root-to-shoot ratios at 2:1 or more in grasslands[60]. Finally, there may be an influence of rising atmospheric CO_2 on biomass, although global trends in CO_2—an ~20% increase since the 1980s—tend to be expressed similarly by region[61].

Our analyses integrated remotely sensed and field-measured levels of annual peak grassland biomass, showing a strong positive relationship despite a tenfold difference in species richness among sites and a hundredfold difference in standing biomass. This indicates that NDVI can capture overall trends in aboveground standing biomass at our sites. Nonetheless, there was widening predictive error as NDVI exceeded 0.6 (Fig. 4). NDVI has been previously shown to accurately predict aboveground plant biomass in uncultivated grasslands[62]. Indeed, we found similar trends of an overall mean biomass increase among our 84 sites for both NDVI and plot-level biomass (Supplementary Fig. 10). However, NDVI can be prone to estimation bias with increasing spatial scale, across years, at higher latitudes and with increasing canopy density and structure[8,53,63]—factors that can characterize some of our data. A fundamental practical question for using NDVI is whether the ability to predict biomass can be improved with widely available ancillary data such as latitude and climate, or whether improvement requires detailed field calibration that may be impossible[16]. Our field data gave us a unique opportunity to test drivers of unexplained variation including fine-scale biotic factors (Methods), revealing two primary sources of bias: high latitude and low elevation. Adding these widely available data to our models improved the predictive accuracy of NDVI for ground-measured biomass by 21% (Supplementary Table 4). Estimation bias at high latitude for NDVI is especially common, relating to methodological and biophysical factors including the potential underestimation of non-photosynthetically active vegetation (which we sampled)[9]. Although our fit between NDVI and aboveground biomass remained strong at higher latitudes,

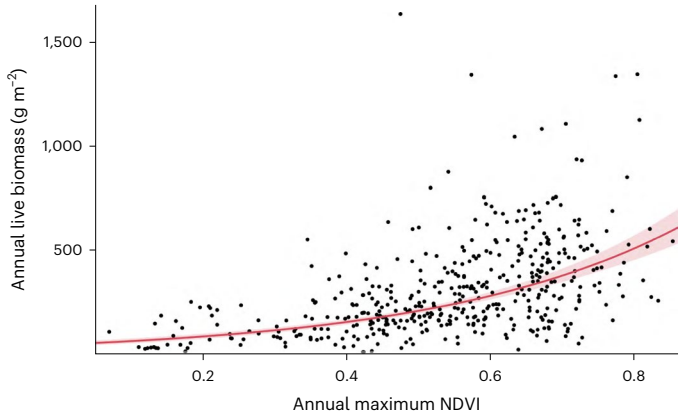

Fig. 4 | Relationship between annual remotely sensed maximum NDVI and annual live aboveground biomass. The best-fit curvilinear regression line ($F_{2,410} = 72.7$; $P < 0.0001$) derives from sites with ≥3 years of live biomass, with the red shaded area (confidence curves for the fitted line) showing how estimation bias begins to widen as the annual maximum NDVI gets higher (especially >0.6). Analysis of the residuals indicates that this bias is strongly affected by higher latitude and lower elevation, with a contribution also from species richness (Methods and Supplementary Table 4).

our work supports the need for caution when extrapolating trends in phenological change including the timing and magnitude of peak biomass. The same caution appears to apply to extrapolating connections among remotely sensed estimates of biomass and species richness[16,64], as we also detected a smaller but significant estimation bias between NDVI and field biomass as the numbers of species per site increased (Supplementary Table 4).

Our work describes a substantial divergence of peak biomass by location within many grasslands globally. These results were obtained from non-cultivated permanent-cover grassland, a habitat type under long-standing and intensifying conversion pressure[53,65]. Despite grassland losses exceeding 99% in some regions[66], uncultivated areas still cover ~25% of Earth's terrestrial surface, store ~25% of its carbon and support thousands of obligate flora and fauna[67]. Many of the global-scale ecological benefits of uncultivated grassland centre on the annual production of biomass, including litter inputs that contribute to soil C cycling, providing forage for much of the world's remaining megafauna and half of all domesticated livestock, and regulating fire cycling given that grasslands account for most of Earth's annual burning[67]. Our documentation of shifts in the direction and magnitude of biomass in our grasslands suggests that there will be far-ranging implications for the planet moving forwards, which will be experienced differently by location.

Methods

Study area and experimental design

Our study sites span a latitudinal gradient from Patagonia (−52°) to the high Arctic of Norway (+78°) and range in elevation from 0 m to 4,241 m, with wide differences in potential evapotranspiration (0.79–6.49 mm per day), atmospheric nitrogen deposition (66.9–2,162.1 mg N m^{-2} per year) and long-term (1970–2020) mean annual precipitation (MAP: 192–2,224 mm) and mean annual temperature (MAT: −7.5 °C to 27.2 °C) (Supplementary Fig. 11 and Table 1). There is wide variation in the total number of species per site ('species richness'), ranging from 13 to 176 species, summed together for all non-treated control plots based on 5 years of sampling in case there were cryptic taxa not visible in some years. The percentage exotic flora ranges from 0 to 100% of all species per site (Supplementary Table 1), with multiple species occurring at sites within both their ancestral and non-native ranges[68]. There were 421 non-native plant taxa in total, but with 20 of the 84 sites having no exotic species (all sites in Europe, Asia and Africa). Levels of grazer offtake at the 46 sites with exclosures range from none to ~85% of total annual plot-level biomass[51,52]. We classify 'grasslands' as low-statured unforested plant communities, including treed savanna, prairie, planted permanent-cover pasture, montane meadows and arctic-alpine tundra. Our sites cover a wide range of 'Whittaker biomes' defined by the ratio of MAP to MAT (Supplementary Fig. 1). They also have some degree of geographic clustering, with an average minimum distance globally of 379.3 km (range: 1 km to 3,087 km). This means that several sites have identical estimates of nitrogen deposition given the spatial resolution of those data (2° × 2.5°). Our ratio of arid-to-mesic grasslands (71%:29%; Supplementary Table 1) matches the global ratio[30], but the continental distribution of our sites is not proportional to the global range of grasslands. Almost half of our sites are from North America even though its continental coverage of grassland is only 13% globally. Australia and South America have similar ratios between number of our sites versus their global coverage (14:13% and 10:9%, respectively), while Asia and Africa are under-represented (Supplementary Fig. 1). For our invaded sites, there could be a concern that our data misrepresent invasion effects on NDVI change because of the gap between the start of the remote sensing data (mid-1980s) and the field sampling (2007). Although we cannot definitively eliminate this possibility (for example, an uninvaded site becoming heavily invaded after 1986), the odds are low as all sites occur in regions of the world with long legacies of invasion dating back a century or more[68]. Our study began with 127 sites, but this number was ultimately reduced to 84 because of screening for extreme outliers, poor image resolution especially due to cloud cover and confounding site factors such as tree cover (see below).

Our analyses combined NDVI calculated from Landsat images starting no earlier than 1986, climate data including PET[35], modelled nitrogen deposition data[36] and field data collected from 84 grassland sites from the Nutrient Network (NutNet), a globally distributed experiment[29]. All NDVI satellite data were extracted from unmodified areas adjacent to plots associated with NutNet (Supplementary Fig. 12). All NutNet plot data were collected by local site scientists, starting in 2007 or later depending on when the site joined the network. Field sampling occurred within 30 permanently marked 5 × 5 m plots laid out in a grid (Supplementary Fig. 12). We used data from the year before the application of any experimental treatment (that is, 'year 0' pre-treatment data, when all plots were unmodified) and from subsequent years (years 1, 2 and so on) in the subset of plots that were untreated (that is, all data in this study come from only unmodified control plots). Plot data were collected annually at peak biomass and included total aboveground biomass, clipped to ground level from two 10 cm × 100 cm strips within a larger 5 m × 5 m plot, with the clipping locations differing each year[29]. Clipped biomass was sorted to live, non-vascular and litter, and then dried to a constant mass at 60 °C and weighed. Differentiating biomass into live vascular, live non-vascular and litter is one of several important novelties of our study, given that the NDVI estimations of standing plant biomass can sometimes be insensitive to, or biased by, the latter two factors. Indeed, 53% of all NutNet grasslands globally have been found to support non-vascular plant growth, with standing biomass as high as 635 g m^{-2} (Virtanen et al., manuscript in preparation).

Our 84 sites captured a wide variation in the relative abundance of major functional groups, including graminoids (for example, grasses and sedges), forbs and, to a lesser degree and mostly in the Arctic, low-statured woody plants, lichens and bryophytes. There was a wide range in the percentage of non-native flora per site. Many sites in Europe, Africa and Asia had few or no non-natives, while some grasslands in North America, South America and Australia were >90% exotic taxa[68]. Species composition data were used to calculate two measures of community-level trait variation, functional diversity and community weighted mean[37]. Functional diversity, an estimate of trait variability, relates to degrees of trait convergence or divergence within

plots based on Rao's index of quadratic entropy. Community weighted mean (also referred to as FI[37]), an estimate of trait averages, is based on the community weighted mean for each trait in each plot. Trait data were compiled from TRY (public version), AusTraits (version 1.1.0), BIEN (version 1.2.5) and NutNet (leaf traits), for six continuous traits (height, leaf surface area (LAI), specific leaf area (ratio of leaf area to leaf mass), leaf N, leaf P and leaf C), that have relatively high coverage for species recorded in NutNet (93%, 95%, 87%, 91%, 86% and 75% for each trait, respectively). For species that do not have trait values, we used the mean values from their genus (Supplementary Table 3).

The only NutNet treatment data were for grazer offtake, derived from fenced but unfertilized plots[51,52]. Grazing effects were expressed as the log response ratio of differences in clipped biomass between control plots in fenced and unfenced areas at a subset of 46 sites (the remaining 38 sites did not have exclosures). Typically, there were three fenced plots per site, and the fences were ~2.3 m tall, with the lower 90 cm being 1 cm steel mesh and the upper portion surrounded by strands of barbless wire[29]. These grazing offtake data were calculated only in the first year after the exclosures were constructed (year 1), given that longer-term exclosure effects can be confounded by shifts in plant species richness and relative abundance[49]. Levels of grazer offtake ranged from very low or nil, with some sites lacking detectable grazing, to very high especially in parts of Australia, Africa and western Europe (for example, sheep grazing in Lancaster, United Kingdom, domesticated reindeer grazing in Kilpisjarvi, Finland)[51,52].

For our analyses, we used single composite (non-temporal) site-level measures of species richness, exotic cover, traits and grazing for each site—this allowed us to test, for example, whether background levels of site richness and invasion were associated with 36 year shifts in NDVI-estimated production.

NDVI measurements and phenological dates

We used images from Landsat missions 4, 5, 7 and 8 to calculate the NDVI at each site, starting as far back as 1986 (depending on image quality) and extending annually to 2020 at a resolution of 30 m in an unmodified circular area selected near the NutNet plots (Supplementary Fig. 12). In these plots, we extracted a series of phenological NDVI measures within each growing season, modified from a previous study[8], given that we targeted only a single vegetation type (that is, grasslands): off-season 'trough' when plants are inactive, start-of-season 'emergence', peak NDVI, end-of-season 'senescence' and 'growing season length' derived from the number of days from emergence to senescence each year (Supplementary Fig. 13). Elsewhere, NDVI has been used to detect trends in phenology and related biomass responses[9,16], including in grasslands where it has been shown to strongly align with live biomass[62]. Our work supports this significant relationship, albeit with increasing variation beyond NDVI values of 0.6 (Fig. 4). We conducted a series of analyses to identify sources of error for NDVI including tests for influences by outliers, the influences of regional-scale factors relating to latitude and elevation, and local-scale factors including non-vascular flora (described below—Supplementary Table 4). We removed two sites that failed uniformity tests when conducting linear fits between annual peak NDVI and time, based on comparisons with a Theil–Sen median regressor and trend filtering using a Mann–Kendall trend test—both were sparsely vegetated sites, of the Icelandic tundra and arid grassland of central North America.

Location of the circular 'NDVI plots' was done visually using Google Earth images. We located a central point in an area adjacent to the NutNet experiment, given that the NutNet plots are readily detectable from the images (Supplementary Fig. 12). This adjacent area was selected to contain vegetation identical to the vegetation within the experiment, in consultation with each NutNet site principle investigator. It was positioned at least 50 m from the closest NutNet plot to avoid the influence of any experimental treatments associated with the NutNet manipulations, while leveraging the site-specific vegetation and soil information derived from the experiment. There is always a potential risk of positioning error using Google Earth—a global analysis of high-resolution Google Earth imagery has estimated an overall horizontal geo-registration accuracy of 39.7 m root mean square error (RMSE) with an accuracy of 24 m RMSE in some countries[69], and subsequent studies show an improved horizontal accuracy of 10.5 m RMSE[70]. We explicitly tested the RSME for 8 of our sites, contrasting plot-level coordinate data generated using a handheld global positioning system at each of 30 plots per site with coordinate data for those same 30 locations generated using Google Earth Engine (Supplementary Fig. 12 and Table 5). Our calculated RSME was always <5 m (Supplementary Table 5).

In each circular plot per site, we extracted reflectance data from within a circular buffer within 30 m around this point (Supplementary Fig. 12). This was done using images from top-of-atmosphere reflectance collections in Google Earth Engine. The images were taken between 1982 and 2020, although the specific date ranges and sampling frequency vary at each site. All of our analyses using remote-sensed data start no earlier than 1986 as site data before this were found to be too sporadic (Supplementary Fig. 13). In all cases, the spatial resolution of each image is 30 m. We used all available images from both tier 1 and tier 2 quality, which were aggregated and processed using Google Earth Engine. Tier 2 data were essential for obtaining images taken during the snow-covered 'trough' portion of the year. The horizontal geo-registration accuracy of tier 1 scenes is ≦12 m RMSE whereas the tier 2 accuracy is >12 m RMSE[71]. Landsat Collection 1 was used, although Collection 2 is the only collection currently available for download, but both collections have the same published geo-registration accuracies[71]. For each image, we calculated NDVI using the corresponding near-infrared and red bands 4 and 3 for Landsat 4, 5 and 6, and bands 5 and 4 for Landsat 8. We also extracted information about image quality (quality assessment band (BQA)) containing statistics from the image data and post-processing information[69]. BQA values were used to filter images to exclude any pixels that had a high likelihood of including clouds or cloud shadows. Using manual inspection, we included only pixels associated with clear, cloud-free imagery (Landsat 4, 5 and 7 BQA = 672, 680, 676, 680 and 684; Landsat 8 BQA = 2,720) or imagery over snow (Landsat 4, 5 and 7 BQA = 1,696, 1,700, 1,704 and 1,708; Landsat 8 BQA = 3,744). We discarded images where resolution was uncertain (for example, clouds versus snow, <0.5% of all images).

We screened our initial pool of sites, reducing the final number of sites to 84 (Supplementary Table 1). Exclusion typically occurred for (1) sites lacking NutNet field data for at least 3 years; (2) sites with extreme outliers for one or more data factors, whose origins could not be determined; or (3) those from which only a minimal amount NDVI phenological data could be extracted. Reasons for the latter include poor satellite coverage by location (especially problematic for Landsat data from the early 1980s), persistent cloud cover (preventing fitting a trend) or sites that rarely or never crossed an identifiable 'greened-up' threshold in multiple years. In cases where established NutNet plots could not be located on Google Earth (Supplementary Fig. 12) or any other issues inhibiting image processing (for example, canopy cover by trees), we reached out to site principal investigators for guidance.

Once the time series of NDVI values was obtained for each site, we extracted key phenological and growing season information by post-processing the data in R version 3.6.1 (Supplementary Fig. 13). First, we smoothed the data to reduce error by fitting cubic splines to the NDVI data at each site, and then determined the average date in which NDVI was the lowest across all years ('trough date'). Then, we created site-specific 'growing season windows' consisting of 545 days ($365 + 2 \times 90$). This window started 90 days before the trough date in each year, and then 365 days following the trough date plus an extra 90 day buffer at the end. We processed all dates initially as radians, which allowed flexibility in defining growing seasons particularly for sites with Mediterranean climates (for example, California, western Australia)

or located in the Southern hemisphere where the period of vegetation activity spans multiple calendar years (for example, green-up can be November of year x, senescence in April of year $x+1$).

From our growing season windows for each site × year combination, we weighted data points so that the maximum NDVI value in each growing season window had a weight of 1, while all other points had a weight of 0.5, to better preserve the NDVI trends at sites with rapid green-ups and short growing seasons. We used a smoothing parameter of 0.5 to preserve these trends. From these annual cubic splines, we extracted green-up and senescence dates as the first and last dates, respectively, that NDVI was above a 50% NDVI range threshold (green threshold) according to the following equation:

$$\text{Threshold} = (0.5 \times (\overline{\text{maximum NDVI}} - \overline{\text{minimum NDVI}})) + \overline{\text{minimum NDVI}}$$

where the average maximum and minimum NDVI values were calculated across all years at each site. This green threshold allowed for the flexibility to include sites with different minimum NDVI values (for example, sites that become snow covered and sites that do not) as well as different maximum NDVI values. In using a threshold, we were also able to ensure that a green-up or senescence date was biologically comparable across all years (indicating the same NDVI).

In all cases of fitting cubic splines, we forced a minimum NDVI value of 0 (if the measured NDVI was <0, we reassigned the value to 0), as our smoothing and post-processing were dependent on consistency during the growing season troughs when data were typically sparse. During the growing season troughs, band quality information often indicated that pixels were cloud covered when visual analysis of images revealed snow cover (both cloud and snow cover containing water). We excluded pixels indicating cloud cover in this analysis. To overcome sparse data points during these periods in tier 1 datasets, we additionally used tier 2 data. Given that data from both tiers were required and the radiometric calibration was top-of-atmosphere reflectance, alternative variations of NDVI that adjust for noise due to soil brightness and atmospheric light scattering, such as the enhanced vegetation index[72,73], were not used—indices with numerical constants can be inconsistent owing to atmospheric noise[69]. Furthermore, snow cover decreases NDVI values but increases enhanced vegetation index values[70] and such sensitivity would confound the phenological analysis.

We approximated the relationship between NDVI and plot-level aboveground biomass using sites with at least 3 years of harvested biomass and corresponding annual peak NDVI data from the same site (Fig. 4 and Supplementary Fig. 10). A log-transformed model provided the best fit between NDVI and average plot biomass per site per year, which we used to translate NDVI to an average biomass across all sites from 1986 to 2020.

Climate and nitrogen deposition trends

Monthly long-term temperature (MAT) and precipitation (MAP) averages per site were obtained from the WorldClim database, from 1970 to 2020. MAT and MAP served to describe baseline levels of temperature and precipitation among sites. To determine annual deviations in temperature and precipitation from baseline MAP and MAT, we calculated a monthly time series for temperature and precipitation during the study period (1986–2020), with data obtained at the site level using the CRU time-series version 4.03 data[35]. These annual deviations were calculated as slopes of change over time. Estimates of potential evapotranspiration were also obtained from the CRU time series[35], which calculates PET using mean, maximum and minimum monthly temperatures, vapour pressure, and cloud cover (1970–2020).

Given predictions of increased inter-annual seasonal variability in climate, with the potential to affect phenology and peak biomass, we calculated slopes of 36 year trends in temperature and precipitation seasonality at each site. We targeted these calculations for two phenophases: (1) green-up based on a 2 month window around the date of typical site-specific green-up date (the typical month of green-up, plus 1 month before) and (2) maximum NDVI as a 5 month window around the date of typical site-specific maximum NDVI (the typical month of maximum NDVI, plus 2 months before and after). These seasonal calculations allowed us to test more detailed climatic drivers of phenological change, which may not be detected by overall annual trends including the possibility of warmer springs, warmer and drier summers, and even seasonal cooling as is sometimes observed[46] (Supplementary Fig. 8).

Atmospheric nitrogen deposition was estimated for each of the sites using the GEOS-Chem Chemical Transport Model[36]. The model estimates wet and dry deposition of inorganic nitrogen using models of atmospheric chemistry together with meteorological data and emission data. Outputs are at a 2° × 2.5° resolution averaged across 2014, 2015 and 2016. Although the nitrogen deposition model uses metrological data, there were weak and non-significant correlations between precipitation and estimates of nitrogen deposition ($r^2 = 0.009$).

Analysis

Our primary analysis tested drivers of change in maximum NDVI over the period starting from 1986 to 2020, based on site-specific slopes of biomass change over time (Fig. 1). We used a multi-model selection approach to evaluate the relative importance of variables associated with our four interacting hypotheses: (1) changes in climate including temperature, precipitation and PET; (2) changes in phenology including the timing of emergence, the timing of senescence and growing season length; (3) levels of atmospheric nitrogen deposition; and (4) biotic factors of species richness, grazing intensity, traits and exotic (non-native) species. We simplified our analytical models by removing factors that were tightly correlated, using principal coordinate analysis (Supplementary Figs. 2 and 3). For example, we found that overall changes in temperature and precipitation (the 36 year temporal trends based on slope) were tightly correlated with seasonal changes in spring and summer temperature and precipitation—we thus used the former in our models. Similarly, sites differed widely in changes to emergence and senescence over time, but we excluded both for our main models as their effects were significantly captured by trends in growing season length—sites that started earlier often had longer growing seasons, as did sites that senesced later (although only 39% of sites had both earlier emergence and later senescence).

Accordingly, we built a maximal linear model in R[74] that assessed the response of site-level biomass slopes (change in NDVI from as early as 1986 to 2020, depending on the site; Fig. 1) to all independent effects and pairwise interactions of a subset of factors: latitude, elevation, nitrogen deposition, species richness, growing season length, aridity, percentage exotic species, overall annual temperature slope (warming since 1986) and overall annual precipitation slope (changes in precipitation since 1986). We included grazing in a separate model for these factors, for the 46 sites that had exclosures (Supplementary Table 2). All of these variables included in the final maximal model had low collinearity, as indicated by assessment of variance inflation factors[75]. These factors also met assumptions of normality (or were log transformed to aid this, for example, nitrogen deposition) and were standardized to a mean of zero and standard deviation of 0.5 using the 'arm' package[76], as required for model comparison[77]. Furthermore, we adjusted our regression models using the inverse of the standard error of the slope from each site, to down-weight parameters estimated with larger error (for example, ref. 78). We evaluated the fit of subsets of this model using the MuMIn package[74] and conducted a model averaging procedure for all candidate models within two Akaike information criterion (AIC) of the best model. We present the full averages of parameter estimates from our final model[75–77] (Table 1 and Supplementary Fig. 2).

Reporting summary

Further information on research design is available in the Nature Portfolio Reporting Summary linked to this article.

Data availability

Data that support the findings of this study are freely available via the Environmental Data Initiative (EDI) Data Portal (https://portal.edirepository.org/nis/advancedSearch.jsp).

Code availability

Code that supports the findings of this study is freely available via the Environmental Data Initiative (EDI) Data Portal (https://portal.edirepository.org/nis/advancedSearch.jsp).

References

1. Nemani, R. R. et al. Climate-driven increases in global terrestrial net primary production from 1982 to 1999. *Science* **300**, 1560–1563 (2003).
2. Ciais, P. et al. Europe-wide reduction in primary productivity caused by the heat and drought in 2003. *Nature* **437**, 529–533 (2005).
3. Zhao, M. & Running, S. W. Drought-induced reduction in global terrestrial net primary production from 2000 through 2009. *Science* **329**, 940–943 (2010).
4. Zhu et al. Greening of the Earth and its drivers. *Nat. Clim. Change* **6**, 791–795 (2016).
5. Running, S. W. et al. A continuous satellite-derived measure of global terrestrial primary production. *Bioscience* **54**, 547–560 (2004).
6. Lobell, D. B., Schlenker, W. & Costa-Roberts, J. Climate trends and global crop production since 1980. *Science* **333**, 616–620 (2011).
7. Tylianakis, J. M. et al. Global change and species interactions in terrestrial ecosystems. *Ecol. Lett.* **11**, 1351–1363 (2008).
8. Buitenwerf, R., Rose, L. & Higgins, S. I. Three decades of multi-dimensional change in global leaf phenology. *Nat. Clim. Change* **5**, 364–368 (2015).
9. Myers-Smith, I. H. et al. Complexity revealed in the greening of the Arctic. *Nat. Clim. Change* **10**, 106–117 (2020).
10. Berner, L. T. et al. Summer warming explains widespread but not uniform greening in the Arctic tundra biome. *Nat. Commun.* **11**, 4621 (2020).
11. Huang, J. et al. Global semi-arid climate change over last 60 years. *Clim. Dyn.* **46**, 1131–1150 (2016).
12. Antar, M. et al. Biomass for a sustainable bioeconomy: an overview of world biomass production and utilization. *Renew. Sustain. Energy Rev.* **139**, 110691 (2021).
13. Krausmann, F. et al. Global human appropriation of net primary production doubled in the 20th century. *Proc. Natl Acad. Sci. USA* **110**, 10324–10329 (2013).
14. Gao, Q. et al. Climatic change controls productivity variation in global grasslands. *Sci. Rep.* **6**, 26958 (2016).
15. Miles, V. V. & Esau, I. Spatial heterogeneity of greening and browning between and within bioclimatic zones in northern West Siberia. *Environ. Res. Lett.* **11**, 115002 (2016).
16. Cavender-Bares, J. et al. Integrating remote sensing with ecology and evolution to advance biodiversity conservation. *Nat. Ecol. Evol.* **6**, 506–519 (2022).
17. Liao, C. et al. Altered ecosystem carbon and nitrogen cycles by plant invasion: a meta-analysis. *New Phytol.* **177**, 706–714 (2008).
18. Turbelin, A. J., Malamud, B. D. & Francis, R. A. Mapping the global state of invasive alien species: patterns of invasion and policy responses. *Glob. Ecol. Biogeogr.* **26**, 78–92 (2017).
19. Borer, E. T. & Stevens, C. J. Nitrogen deposition and climate: an integrated synthesis. *Trends Ecol. Evol.* **6**, 541–552 (2022).
20. Knapp, A. K., Ciais, P. & Smith, M. D. Reconciling inconsistencies in precipitation–productivity relationships: implications for climate change. *New Phytol.* **214**, 41–47 (2017).
21. Teng, M. et al. The impacts of climate changes and human activities on net primary productivity vary across an ecotone zone in Northwest China. *Sci. Total Environ.* **714**, 136691 (2020).
22. Zani, D. et al. Increased growing-season productivity drives earlier autumn leaf senescence in temperate trees. *Science* **370**, 1066–1071 (2020).
23. Luo, Y. et al. Nutrients and water availability constrain the seasonality of vegetation activity in a Mediterranean ecosystem. *Glob. Change Biol.* **26**, 4379–4400 (2020).
24. Walker, M. D. et al. Plant community responses to experimental warming across the tundra biome. *Proc. Natl Acad. Sci. USA* **103**, 1342–1346 (2006).
25. Parmesan, C. & Hanley, M. E. Plants and climate change: complexities and surprises. *Ann. Bot.* **106**, 849–864 (2015).
26. Olofsson, J. et al. Herbivores inhibit climate-driven shrub expansion on the tundra. *Glob. Change Biol.* **15**, 2681–2693 (2009).
27. Maestre, F. T. et al. Grazing and ecosystem service delivery in global drylands. *Science* **378**, 915–920 (2022).
28. Yahdjian, L. et al. Why coordinated distributed experiments should go global. *BioScience* **71**, 918–927 (2021).
29. Borer, E. T. et al. Finding generality in ecology: a model for globally distributed experiments. *Methods Ecol. Evol.* **5**, 65–73 (2014).
30. White, R. P., Murray, S., Rohweder, M., Prince, S. D. & Thompson, K. M. *Grassland Ecosystems* (World Resources Institute, 2000).
31. Axelrod, D. I. Rise of the grassland biome, central North America. *Bot. Rev.* **51**, 163–201 (1985).
32. Sala, O. E. et al. Primary production of the central grassland region of the United States. *Ecology* **69**, 40–45 (1988).
33. Knapp, A. K. & Smith, M. D. Variation among biomes in temporal dynamics of aboveground primary production. *Science* **291**, 481–484 (2001).
34. Gilbert, B. et al. Climate and local environment structure asynchrony and the stability of primary production in grasslands. *Glob. Ecol. Biogeogr.* **7**, 1177–1188 (2020).
35. Harris, I., Osborn, T. J., Jones, P. & Lister, D. Version 4 of the CRU TS monthly high-resolution gridded multivariate climate dataset. *Sci. Data* **7**, 109 (2020).
36. Ackerman, D., Millet, D. B. & Chen, X. Global estimates of inorganic nitrogen deposition across four decades. *Global Biogeochem. Cy.* **33**, 100–107 (2019).
37. van der Plas, F. et al. Plant traits alone are poor predictors of ecosystem properties and long-term ecosystem functioning. *Nat. Ecol. Evol.* **4**, 1602–1611 (2020).
38. Heisler-White, J. L., Knapp, A. K. & Kelly, E. F. Increasing precipitation event size increases aboveground net primary productivity in a semi-arid grassland. *Oecologia* **158**, 129–140 (2008).
39. Xia, J. et al. Spatio-temporal patterns and climate variables controlling of biomass carbon stock of global grassland ecosystems from 1982 to 2006. *Remote Sens.* **6**, 1783–1802 (2014).
40. Orndahl, K. M., Macander, M. J., Berner, L. T. & Goetz, S. J. Plant functional type aboveground biomass change within Alaska and northwest Canada mapped using a 35-year satellite time series from 1985 to 2020. *Environ. Res. Lett.* **17**, 115010 (2022).
41. Boone, R. B., Conant, R. T., Sircely, J., Thornton, P. K. & Herrero, M. Climate change impacts on selected global rangeland ecosystem services. *Glob. Change Biol.* **24**, 1382–1393 (2018).
42. Andresen, L. C. et al. Biomass responses in a temperate European grassland through 17 years of elevated CO_2. *Glob. Change Biol.* **24**, 3875–3885 (2018).
43. MacDougall, A. S. et al. Comparison of the distribution and phenology of Arctic mountain plants between the early 20th and 21st centuries. *Glob. Change Biol.* **27**, 5070–5083 (2021).
44. Möhl, P., von Büren, R. S. & Hiltbrunner, E. Growth of alpine grassland will start and stop earlier under climate warming. *Nat. Commun.* **13**, 7398 (2022).

45. Friedman, A. R. et al. Interhemispheric temperature asymmetry over the twentieth century and in future projections. *J. Clim.* **26**, 5419–5433 (2013).
46. MacDougall, A. S., Wilson, S. D. & Bakker, J. D. Climatic variability alters the outcome of long-term community assembly. *J. Ecol.* **96**, 346–354 (2008).
47. Grace, J. B. et al. Integrative modelling reveals mechanisms linking productivity and plant species richness. *Nature* **529**, 390–393 (2016).
48. Anderson, T. M. et al. Herbivory and eutrophication mediate grassland plant nutrient responses across a global climatic gradient. *Ecology* **99**, 822–831 (2018).
49. Dee, L. E. et al. Clarifying the effect of biodiversity on productivity in natural ecosystems with longitudinal data and methods for causal inference. *Nat. Commun.* **14**, 2607 (2023).
50. Seabloom, E. W. et al. Plant species' origin predicts dominance and response to nutrient enrichment and herbivores in global grasslands. *Nat. Commun.* **6**, 7710 (2015).
51. Borer, E. T. et al. Herbivores and nutrients control grassland plant diversity via light limitation. *Nature* **508**, 517–520 (2014).
52. Borer, E. T. et al. Nutrients cause grassland biomass to outpace herbivory. *Nat. Commun.* **11**, 6036 (2020).
53. Delegido, J. et al. A red-edge spectral index for remote sensing estimation of green LAI over agroecosystems. *Eur. J. Agron.* **46**, 42–52 (2013).
54. Eisfelder, C. et al. Above-ground biomass estimation based on NPP time-series—a novel approach for biomass estimation in semi-arid Kazakhstan. *Ecol. Indic.* **72**, 13–22 (2017).
55. Donat, M. G., Lowry, A. L., Alexander, L. V., O'Gorman, P. A. & Maher, N. More extreme precipitation in the world's dry and wet regions. *Nat. Clim. Change* **6**, 508–513 (2016).
56. Zeng, X. et al. The global decline in the sensitivity of vegetation productivity to precipitation from 2001 to 2018. *Glob. Change Biol.* **28**, 6823–6833 (2022).
57. Clay, D. E. et al. Does the conversion of grasslands to row crop in semi-arid areas threaten global food supplies? *Glob. Food Secur.* **3**, 22–30 (2014).
58. Godde, C. M. et al. Global rangeland production systems and livelihoods at threat under climate change and variability. *Environ. Res. Lett.* **15**, 044021 (2020).
59. Jackson, R. B., Banner, J. L., Jobbágy, E. G., Pockman, W. T. & Wall, D. H. Ecosystem carbon loss with woody plant invasion of grasslands. *Nature* **418**, 623–626 (2002).
60. Cleland, E. E. et al. Belowground biomass response to nutrient enrichment depends on light limitation across globally distributed grasslands. *Ecosystems* **7**, 1466–1477 (2019).
61. Hungate, B. A. et al. The fate of carbon in grasslands under carbon dioxide enrichment. *Nature* **388**, 576–579 (1997).
62. Chen, M. et al. Assessing precipitation, evapotranspiration, and NDVI as controls of US Great Plains plant production. *Ecosphere* **10**, e02889 (2019).
63. Jiang, Z. et al. Analysis of NDVI and scaled difference vegetation index retrievals of vegetation fraction. *Remote Sens. Environ.* **101**, 366–378 (2006).
64. Rocchini, D., Ricotta, C. & Chiarucci, A. Using satellite imagery to assess plant species richness: the role of multispectral systems. *Appl. Veg. Sci.* **10**, 325–331 (2007).
65. Kong, L. et al. Natural capital investments in China undermined by reclamation for cropland. *Nat. Ecol. Evol.* **7**, 1771–1777 (2023).
66. Goldewijk, K. K. Estimating global land use change over the past 300 years: the HYDE database. *Glob. Biogeochem. Cycles* **15**, 417–433 (2001).
67. Lehmann, C. E. et al. Savanna vegetation–fire–climate relationships differ among continents. *Science* **343**, 548–552 (2014).
68. Firn, J. et al. Abundance of introduced species at home predicts abundance away in herbaceous communities. *Ecol. Lett.* **14**, 274–281 (2011).
69. Potere, D. Horizontal positional accuracy of Google Earth's high-resolution imagery archive. *Sensors* **8**, 7973–7981 (2008).
70. Salinas-Castillo, W. E. & Paredes-Hernández, C. U. Horizontal and vertical accuracy of Google Earth®: comment on 'Positional accuracy of the Google Earth terrain model derived from stratigraphic unconformities in the Big Bend region, Texas, USA' by S.C. Benker, R.P. Langford and T.L. Pavlis. *Geocarto Int.* **29**, 625–627 (2014).
71. Landsat Collection 1. *United States Geological Survey (USGS)* https://www.usgs.gov/landsat-missions/landsat-collection-1 (2023).
72. Huete, A. et al. Overview of the radiometric and biophysical performance of the MODIS vegetation indices. *Remote Sens. Environ.* **83**, 195–213 (2002).
73. Young, A. T. Rayleigh scattering. *Appl. Opt.* **20**, 533–535 (1981).
74. R Core Team. R: A language and environment for statistical computing; https://www.R-project.org/ (R Foundation for Statistical Computing, 2021).
75. Zuur, A. F., Ieno, E. N. & Elphick, C. S. A protocol for data exploration to avoid common statistical problems. *Methods Ecol. Evol.* **1**, 3–14 (2010).
76. Gelman, A. arm: Data analysis using regression and multilevel/ hierarchical models; http://cran.r-project.org/web/packages/arm (2011).
77. Grueber, C. E., Nakagawa, S., Laws, R. J. & Jamieson, I. G. Multi-model inference in ecology and evolution: challenges and solutions. *J. Evol. Biol.* **24**, 699–711 (2011).
78. Seabloom, E. W. et al. Species loss due to nutrient addition increases with spatial scale in global grasslands. *Ecol. Lett.* **24**, 2100–2112 (2021).

Acknowledgements

We thank each of the researchers who have contributed data and ideas to the NutNet (http://www.nutnet.org). Grants to A.S.M., E.E., C.B. and O.C. came from the University of Guelph's Canada First Research Excellence Fund project 'Food from Thought'. Thank you to S. Rodrigues for technical support on data extraction from Google Earth and A. Bjorkman for comments on the paper. Fieldwork was funded at the site scale by individual researchers. Coordination and data management in the NutNet have been supported by funding to E.T.B. and E.W.S. from the National Science Foundation Research Coordination Network (NSF-DEB-1042132) and Long-Term Ecological Research (NSF-DEB-1234162 to Cedar Creek LTER) programmes, and the Institute on the Environment (DG-0001-13). We also thank the Minnesota Supercomputer Institute for hosting project data and the Institute on the Environment for hosting network meetings. This study was funded by the Canada First Research Excellence Fund—University of Guelph ('Food From Thought'), Natural Sciences and Engineering Research Council of Canada (A.S.M.), National Science Foundation Research Coordination Network (NSF-DEB-1042132) and Long Term Ecological Research (NSF-DEB-1234162 to Cedar Creek LTER).

Author contributions

Conceptualization: A.S.M., E.E. with M.S., C.B., K.L. and J.O. Methodology: E.E. with A.S.M., O.C., C.B., Q.C., E.W.S., T.O. and E.T.B. Investigation: E.E. and A.S.M. Visualization: A.S.M. and E.E. Analyses: A.S.M., with O.C., C.B., E.E., T.O., E.W.S. and Q.C. Funding acquisition: A.S.M., with E.T.B. and E.W.S. Project administration: A.S.M. Supervision: A.S.M. Writing—original draft: A.S.M. with E.E. Writing—review and editing: A.S.M., E.E. and all co-authors. Data collection and contribution: all co-authors.

Andrew S. MacDougall[1,2] ✉, Ellen Esch[1], Qingqing Chen[3], Oliver Carroll[1], Colin Bonner[1], Timothy Ohlert[4], Matthias Siewert[2], John Sulik[5], Anna Schweiger[6], Elizabeth T. Borer[7], Dilip Naidu[8], Sumanta Bagchi[8], Yann Hautier[9], Peter Wilfahrt[7], Keith Larson[2], Johan Olofsson[2], Elsa Cleland[10], Ranjan Muthukrishnan[11], Lydia O'Halloran[12], Juan Alberti[13], T. Michael Anderson[14], Carlos A. Arnillas[15], Jonathan D. Bakker[16], Isabel C. Barrio[17], Lori Biederman[18], Elizabeth H. Boughton[19], Lars A. Brudvig[20], Martin Bruschetti[13], Yvonne Buckley[21], Miguel N. Bugalho[22], Marc W. Cadotte[23], Maria C. Caldeira[24], Jane A. Catford[25], Carla D'Antonio[26], Kendi Davies[27], Pedro Daleo[13], Christopher R. Dickman[28], Ian Donohue[21], Mary Ellyn DuPre[29], Kenneth Elgersma[30], Nico Eisenhauer[31,32], Anu Eskelinen[31,33,34], Catalina Estrada[35], Philip A. Fay[36], Yanhao Feng[37], Daniel S. Gruner[38], Nicole Hagenah[39], Sylvia Haider[40], W. Stanley Harpole[31,33,41], Erika Hersch-Green[42], Anke Jentsch[43], Kevin Kirkman[44], Johannes M. H. Knops[45], Lauri Laanisto[46], Lucíola S. Lannes[47], Ramesh Laungani[48], Ariuntsetseg Lkhagva[49], Petr Macek[50], Jason P. Martina[51], Rebecca L. McCulley[52], Brett Melbourne[27], Rachel Mitchell[53], Joslin L. Moore[54,55,56], John W. Morgan[57], Taofeek O. Muraina[58,74], Yujie Niu[42,59], Meelis Pärtel[60], Pablo L. Peri[61], Sally A. Power[62], Jodi N. Price[63], Suzanne M. Prober[64], Zhengwei Ren[65], Anita C. Risch[66], Nicholas G. Smith[67], Grégory Sonnier[19], Rachel J. Standish[68], Carly J. Stevens[69], Michelle Tedder[43], Pedro Tognetti[70], G. F. (Ciska) Veen[71], Risto Virtanen[34], Glenda M. Wardle[28], Elizabeth Waring[72], Amelia A. Wolf[73], Laura Yahdjian[70] & Eric W. Seabloom[7]

[1]Department of Integrative Biology, University of Guelph, Guelph, Ontario, Canada. [2]Department of Ecology and Environmental Sciences, Umeå University, Umeå, Sweden. [3]Institute of Ecology, College of Urban and Environmental Science, Peking University, Beijing, China. [4]Department of Biology, University of New Mexico, Albuquerque, NM, USA. [5]Department of Plant Agriculture, University of Guelph, Guelph, Ontario, Canada. [6]Land Resources and Environmetal Sciences, Montana State University, Bozeman, MT, USA. [7]Department of Ecology, Evolution, and Behavior, University of Minnesota, Saint Paul, MN, USA. [8]Centre for Ecological Sciences, Indian Institute of Science, Bangalore, India. [9]Ecology and Biodiversity Group, Department of Biology, Utrecht University, Utrecht, The Netherlands. [10]Division of Biological Sciences, University of California, San Diego, San Diego, CA, USA. [11]Department of Biology, Boston University, Boston, MA, USA. [12]Baruch Institute of Coastal Ecology and Forest Science, Clemson University, Clemson, SC, USA. [13]Instituto de Investigaciones Marinas y Costeras (IIMyC) FCEyN, UNMdP-CONICET, Mar del Plata, Argentina. [14]Department of Biology, Wake Forest University, Winston-Salem, NC, USA. [15]Department of Physical and Environmental Sciences, University of Toronto—Scarborough, Toronto, Ontario, Canada. [16]School of Environmental and Forest Sciences, University of Washington, Seattle, WA, USA. [17]Faculty of Environmental and Forest Sciences, Agricultural University of Iceland, Reykjavik, Iceland. [18]Department of Ecology, Evolution, and Organismal Biology, Iowa State University, Ames, IA, USA. [19]Archbold Biological Station, Venus, FL, USA. [20]Department of Plant Biology and Program in Ecology, Evolution, and Behavior, Michigan State University, East Lansing, MI, USA. [21]Department of Zoology, School of Natural Sciences, Trinity College Dublin, Dublin, Ireland. [22]Centre for Applied Ecology, School of Agriculture, University of Lisbon, Lisbon, Portugal. [23]Department of Biological Sciences, University of Toronto—Scarborough, Toronto, Ontario, Canada. [24]Forest Research Centre, School of Agriculture, University of Lisbon, Lisbon, Portugal. [25]Department of Geography, King's College London, London, UK. [26]Department of Ecology, Evolution, and Marine Biology, University of California, Santa Barbara, Santa Barbara, CA, USA. [27]Department of Ecology and Evolutionary Biology, University of Colorado, Boulder, CO, USA. [28]School of Life and Environmental Sciences, University of Sydney, Camperdown, New South Wales, Australia. [29]MPG Ranch, Missoula, MT, USA. [30]University of Northern Iowa, Cedar Falls, IA, USA. [31]German Centre for Integrative Biodiversity Research (iDiv) Halle-Jena-Leipzig, Leipzig, Germany. [32]Institute of Biology, Leipzig University, Leipzig, Germany. [33]Department of Physiological Diversity, Helmholtz Centre for Environmental Research—UFZ, Leipzig, Germany. [34]Department of Ecology and Genetics, University of Oulu, Oulu, Finland. [35]Department of Life Sciences, Imperial College London, Ascot, UK. [36]USDA-ARS Grassland Soil, and Water Research Laboratory, Temple, TX, USA. [37]College of Pastoral Agriculture Science and Technology, Lanzhou University, Lanzhou, China. [38]Department of Entomology, University of Maryland, College Park, MD, USA. [39]Department of Zoology & Entomology, University of Pretoria, Pretoria, South Africa. [40]Institute of Ecology, Leuphana University of Lüneburg, Lüneburg, Germany. [41]Martin Luther University Halle-Wittenberg, Halle (Saale), Germany. [42]Department of Biological Sciences, Michigan Technological University, Houghton, MI, USA. [43]Department of Disturbance Ecology, Bayreuth Center of Ecology and Environmental Research, University of Bayreuth, Bayreuth, Germany. [44]School of Life Sciences, College of Agriculture, Engineering and Science, University of KwaZulu-Natal, Durban, South Africa. [45]Department of Health and Environmental Sciences, Jiatong–Liverpool University, Suzhou, China. [46]Chair of Biodiversity and Nature Tourism,

Estonian University of Life Sciences, Tartu, Estonia. [47]Department of Biology and Animal Sciences, Sao Paulo State University UNESP, Ilha Solteira, Brazil. [48]Department of Environmental Science and Policy, Marist College, Poughkeepsie, NY, USA. [49]Department of Biology, National University of Mongolia, Ulaanbaatar, Mongolia. [50]Institute of Hydrobiology, Biology Centre of Czech Academy of Sciences, Ceske Budejovice, Czech Republic. [51]Department of Biology, Texas State University, San Marcos, TX, USA. [52]Department of Plant and Soil Sciences, University of Kentucky, Lexington, KY, USA. [53]School of Earth and Sustainability, Northern Arizona University, Flagstaff, AZ, USA. [54]Arthur Rylah Institute for Environment Research, Department of Energy Environment and Climate Action, Melbourne, Victoria, Australia. [55]School of Biological Sciences, Monash University, Clayton, Victoria, Australia. [56]School of Agriculture, Food and Ecosystem Sciences, The University of Melbourne, Melbourne, Victoria, Australia. [57]Department of Environment and Genetics, La Trobe University, Bundoora, Victoria, Australia. [58]Department of Animal Health and Production, Oyo State College of Agriculture and Technology, Igbo-Ora, Nigeria. [59]College of Grassland Science, Key Laboratory of Grassland Ecosystem of the Ministry of Education, Gansu Agricultural University, Lanzhou, China. [60]Institute of Ecology and Earth Sciences, University of Tartu, Tartu, Estonia. [61]INTA-UNPA-CONICET, Universidad Nacional de la Patagonia, Rìo Gallegos, Argentina. [62]Hawkesbury Institute for the Environment, Western Sydney University, Penrith, New South Wales, Australia. [63]Gulbali Institute, Charles Sturt University, Albury, New South Wales, Australia. [64]CSIRO Environment, Canberra, Australian Capital Territory, Australia. [65]College of Ecology, Lanzhou University, Lanzhou, China. [66]Swiss Federal Institute for Forest Snow and Landscape Research WSL, Birmensdorf, Switzerland. [67]Department of Biological Sciences, Texas Tech University, Lubbock, TX, USA. [68]Murdoch University, Perth, Western Australia, Australia. [69]Lancaster Environment Centre, Lancaster University, Lancaster, UK. [70]IFEVA Facultad de Agronomía, Universidad de Buenos Aires–CONICET, Buenos Aires, Argentina. [71]Department of Terrestrial Ecology, Netherlands Institute of Ecology, Wageningen, The Netherlands. [72]Department of Natural Sciences, Northeastern State University, Tahlequah, OK, USA. [73]Department of Integrative Biology, University of Texas at Austin, Austin, TX, USA. [74]Present address: Department of Biology, Texas State University, San Marcos, TX, USA. ✉e-mail: asm@uoguelph.ca